Naval Research Laboratory

Washington, DC 20375-5320

NRL/MR/6394--19-9906

Basis Functions for Parametric Modeling of Energy-Deposition Processes

Samuel G. Lambrakos

Center for Computational Materials Science
Materials Science and Technology Division

September 5, 2019

REPORT DOCUMENTATION PAGE

Form Approved
OMB No. 0704-0188

1. REPORT DATE *(DD-MM-YYYY)*	**2. REPORT TYPE**	**3. DATES COVERED** *(From - To)*
06-09-2019	NRL Memorandum Report	

4. TITLE AND SUBTITLE

Basis Functions for Parametric Modeling of Energy-Deposition Processes

5a. CONTRACT NUMBER

5b. GRANT NUMBER

5c. PROGRAM ELEMENT NUMBER

6. AUTHOR(S)

Samuel G. Lambrakos

5d. PROJECT NUMBER
63-1G69-09

5e. TASK NUMBER

5f. WORK UNIT NUMBER
1G69

7. PERFORMING ORGANIZATION NAME(S) AND ADDRESS(ES)

Naval Research Laboratory
4555 Overlook Avenue, SW
Washington, DC 20375-5320

8. PERFORMING ORGANIZATION REPORT NUMBER

NRL/MR/6394--19-9906

9. SPONSORING / MONITORING AGENCY NAME(S) AND ADDRESS(ES)

Office of Naval Research
One Liberty Center
875 North Randolph Street, Suite 1425
Arlington, VA 22203-1995

10. SPONSOR / MONITOR'S ACRONYM(S)

ONR

11. SPONSOR / MONITOR'S REPORT NUMBER(S)

12. DISTRIBUTION / AVAILABILITY STATEMENT

DISTRIBUTION STATEMENT A: Approved for public release distribution is unlimited.

13. SUPPLEMENTARY NOTES

14. ABSTRACT

A methodology is extended for inverse thermal analysis of energy-deposition processes. This methodology is in terms of numerical-analytical basis functions and equivalent source distributions, and provides relatively optimal parametric modeling of temperature fields associated with energy deposition processes. The methodology's extension is by construction of numerical-analytical basis functions, based on the concepts of effective diffusion and effective advection. This extension permits parameter optimization with respect to different types of workpiece boundary conditions, energy-deposition processes, and temperature-field constraints based on measurements.

15. SUBJECT TERMS

Inverse analysis Parametric modeling
Energy deposition

16. SECURITY CLASSIFICATION OF:			**17. LIMITATION OF ABSTRACT**	**18. NUMBER OF PAGES**	**19a. NAME OF RESPONSIBLE PERSON**
					Samuel G. Lambrakos
a. REPORT	**b. ABSTRACT**	**c. THIS PAGE**	Unclassified Unlimited	22	**19b. TELEPHONE NUMBER** *(include area code)*
Unclassified Unlimited	Unclassified Unlimited	Unclassified Unlimited			(202) 767-2601

Standard Form 298 (Rev. 8-98)
Prescribed by ANSI Std. Z39.18

This page intentionally left blank.

Contents

This page intentionally left blank.

Introduction

Previous studies introduced and demonstrated inverse thermal analysis of heat-deposition processes using a methodology based on numerical-analytical basis functions and equivalent source distributions [1-8]. These studies discuss aspects of the methodology concerning parameter optimization, properties related to signal-processing, and the ability of inverse models to compensate for lack of information concerning material properties. Reference [1] discusses historical classification of this methodology with respect to the general inverse heat transfer problem (IHTP). In particular, that inverse thermal analysis of energy deposition in plate structures, may be classified as the IHTP of either boundary conditions or source terms. This follows in that selection of a parameterized source function is actually equivalent to selection of a surface generator for a temperature-field boundary within the bounded spatial domain defined by the workpiece. A general approach for inverse thermal analysis follows from observations that material response to energy deposition may be encoded onto parameters associated with discrete energy-source distributions in space. These spatial distributions of discrete sources do not represent "local" parameterization of the energy coupling, but rather the integrated power deposition, which is with respect to space and time, within specified boundaries, e.g., solidification boundaries (in general, transformation boundaries) or isothermal boundaries that are defined by temperature measurements, e.g., thermocouple measurements.

As discussed previously [1-8], the formal structure underlying the methodology is that of parametric modeling of temperature fields using numerical-analytical basis functions (NABFs) and equivalent source distributions (ESDs). This methodology is motivated by references [9-11], and provides reduction of model complexity for purposes of inverse thermal analysis. This report presents extension of the methodology for inverse thermal analysis of energy-deposition processes with respect to its formulation. The extension is by inclusion of generalized numerical-analytical basis functions.

For processes involving energy deposition within finite volumes of material, parametric representations of temperature fields are linear combinations of NABFs given by

Manuscript approved August 5, 2019.

$$T(\hat{x},t) = T_A + \sum_{k=1}^{N_k}\sum_{n=1}^{N_t} C(\hat{x}_k)F_A(\hat{x},\hat{x}_k,\hat{\kappa},n\Delta t - t_k,V)$$

$$+\sum_{k=1}^{N_k} C(\hat{x}_k)F_B(\hat{x},\hat{x}_k,\hat{\kappa},V) \qquad \text{(Eq 1)}$$

where

$$F_A(\hat{x},\hat{x}_k,\hat{\kappa},t,V) = T_1(x-Vt,x_k,\kappa_1,t)T_2(y,y_k,\kappa_2,t)T_3(z,z_k,\kappa_3,t)\,, \qquad \text{(Eq 2)}$$

the functions F_B are analytical solutions of the steady-state heat conduction equation, and

$$t = \frac{x}{V} \qquad \text{(Eq 3)}$$

The basis functions making up the linear combination defined by Eq.(1) include dependence on the effective-diffusion vector $\hat{\kappa} = (\kappa_1,\kappa_2,\kappa_3)$. The temperature fields T_i (i=1,2,3) of Eqs. (2) are solutions of the one-dimensional heat conduction equation

$$\frac{\partial T_i}{\partial t} = \kappa_i \frac{\partial^2 T_i}{\partial x_i^2} \quad , \qquad \text{(Eq 4)}$$

for initial conditions

$$T_i(x_i,x_{i,k},\kappa_i,0) = \delta(x_i - x_{i,k})\,, \qquad \text{(Eq 5)}$$

The basis functions F_B are solutions of the three-dimensional steady-state heat conduction equation

$$\kappa\nabla^2 T + V\frac{\partial T}{\partial x} = 0, \qquad \text{(Eq 6)}$$

for initial conditions

$$T(\hat{x},\hat{x}_k,\hat{\kappa}) = \delta(\hat{x} - \hat{x}_k), \qquad \text{(Eq 7)}$$

where the heat source is moving along the x-coordinate in the positive direction with velocity V.

The discrete equivalent source distribution $C(\hat{x}_k)$ given in Eqs. (1) are such that for constraint conditions

$$T(\hat{x}_n^c,t_n^c) = T_n^c \quad , \qquad \text{(Eq 8)}$$

values of the objective function

$$Z_T = \sum_{n=1}^{N} w_n \left(T(\hat{x}_n^c, t_n^c) - T_n^c \right)^2 \quad \text{(Eq 9)}$$

satisfy the condition

$$Z_T \le \varepsilon \quad \text{(Eq 10)}$$

for a specified value of ε. The qunatity T_n^c is the target temperature for position $\hat{x}_n^c = (x_n^c, y_n^c, z_n^c)$. The quantities w_n ($n=1,...,N$) are weight coefficients that specify relative levels of influence associated with constraint conditions T_n^c. It follows that $T(\hat{x}, \hat{x}_k, \hat{\kappa}, t)$ can constructed using combinations of general forms of the solution to the heat conduction equation, which are as follows.

First, the heat kernel and the Fourier series solutions of Eq. (4) for an unbounded region and region having nonconduction boundaries [12], given by

$$T_i(x_i, x_{ik}, \kappa_i, t) = \frac{1}{\sqrt{t}} \exp\left[-\frac{(x_i - x_{ik})^2}{4\kappa_i t} \right], \quad \text{(Eq 11)}$$

and

$$T_i(x_i, x_{ik}, \kappa_i, t) = \left\{ 1 + 2\sum_{m=1}^{\infty} \exp\left[-\frac{\kappa_i m^2 \pi^2 t}{l^2} \right] \cos\left[\frac{m\pi x_i}{l} \right] \cos\left[\frac{m\pi x_{ik}}{l} \right] \right\}, \quad \text{(Eq 12)}$$

respectively. Although given in many studies, for completeness with respect to development of the methodology considered here, differents forms of solutions to the heat conduction equation are given in Appendix 1, which include a Fourier-series solution that is equivalent to Eq.(11).

Next, solution of Eq. (6) for an unbounded system and heat source of unit strength, at (x_k, y_k, z_k), is given by

$$T(\hat{x}, \hat{x}_k) = \frac{1}{4\pi k r} \exp\left[-\frac{V}{2\kappa} (r + x - x_k) \right] \quad \text{(Eq 13)}$$

where

$$r = \sqrt{(x - x_k)^2 + (y - y_k)^2 + (z - z_k)^2} \quad \text{(Eq 14)}$$

and k is the thermal conductivity. And finally, solution of Eq.(6) for a line-source of unit strength at (x_k, y_k) moving along the x-coordinate in the positive direction with velocity V, within a workpiece of thickness d (having nonconducting surface boundaries), is given by

$$T(x, x_k, y, y_k) = \frac{1}{2\pi kd} \exp\left[-\frac{V}{2\kappa}(x - x_k)\right] K_0\left(\frac{Vr}{2\kappa}\right) \qquad \text{(Eq 15)}$$

where

$$r = \sqrt{(x - x_k)^2 + (y - y_k)^2} \qquad \text{(Eq 16)}$$

and K_0 is the modified bessel function of the second kind. Given in the appendix for completeness, is the Fourier-series solution of Eq.(4) that is equivalent to Eq.(11), from which Eq. (12) is derived. In what follows, the terms of Eq.(1) defined by Eqs. (11)-(16) are extended parametrically to include dependence on the effective-diffusion vector $\hat{\kappa} = (\kappa_1, \kappa_2, \kappa_3)$ and the effective-advection vector $\boldsymbol{V} = (V_1, V_2, V_3)$.

The quantity T_A is the ambient temperature of the workpiece and the locations $\hat{x}_n^c$ and temperature values T_n^c specify constraint conditions on the temperature field. Constraint conditions are imposed on the temperature field spanning the spatial domain of interest within the workpiece by minimization of the objective function defined by Eq. (9), where T_n^c is the target temperature for position $\hat{x}_n^c = (x_n^c, y_n^c, z_n^c)$. The input of information into the inverse model defined by Eqs. (1)-(3), (8) and (9) is effected by the assignment of individual constraint values to the quantities T_n^c and the form of the basis functions adopted for parametric representation, which include boundary conditions. The constraint conditions, i.e., $T(\hat{x}_n^c, t_n^c) = T_n^c$, and basis functions provide for the inclusion of information from both laboratory and numerical experiments. Equations (1)-(3), (8) and (9) specify a general procedure for inverse thermal analysis.

As emphasized in reference [1], inverse thermal analysis using NABFs and ESDs adopts the analysis approach of signal processing, where a system's response, no matter how complex, is decomposed using linear combinations of component contributions, whose formal structure are characteristic modes of that system. For

the case of inverse thermal analysis, these characteristic modes are the solutions to the heat conduction equation, representing the simplest parametrization in terms of basis functions.

Reference [1] presents a rigorous analysis of local-to-far field filtering associated with heat diffusion. In particular, that a fundamental property of source distributions $C(x_k)$ is that their detailed structure has essentially no influence on the calculated temperature field for spatial locations sufficiently far field relative to the energy-source location. In that calculated temperature fields are insensitive to details of source distributions at sufficiently far field, source distributions can be of minimal complexity, thus conveniently adjustable. Further, one can calculate temperature fields using different types of numerical-analytical basis functions. In particular, parametric modeling of steady-state heat deposition within plate structures entails using local-to-far field mappings of upstream source distributions to downstream temperature fields. Accordingly, temperature fields within plate structures, characterized by finite thickness, become independent of the z-coordinate within downstream regions, as well as details of source distributions transverse to their motion.

The methodology applies two types of ESDs (see Fig. 1). One is that of discrete sources distributed volumetrically, having specified strengths, and the other of discrete sources distributed volumetrically, having both specified strengths and effective-diffusion vectors. Which of these ESDs is more convenient for inverse thermal analysis, as well as ESDs combining the two types, should depend on the heat deposition process considered for inverse thermal analysis. For heat-deposition characterized volumetrically by relatively simple shapes, e.g., laser and electron beam welding, ESDs having specified strengths alone should be sufficiently convenient for parametric modeling. In constrast, for heat-deposition processes, where energy deposition is characterized by complex shapes, ESDs having specified strengths and effective-diffusion vectors should be more convenient for parametric modeling. The basis functions are for frames of reference that are fixed to moving source distributions, representing the quasi-steady-state condition for energy deposition (see Fig. 2 top). Another set of basis functions considers energy deposition for frames of reference that are fixed to the workpiece (see Fig.

2 bottom). As described below, the concept of effective-diffusion vectors can be extended to that of effective-advection vectors.

Energy-deposition characterized by complex shapes, which can include combinations of heat sources and complex material flow patterns, can be modeled by NABFs and ESDs whose parameterizations include effective-diffusion vectors $\hat{\kappa} = (\kappa_1, \kappa_2, \kappa_3)$. This parameterization is based on replacing the advection-diffusion operator with an effective-diffusion operator, i.e.,

$$\kappa \nabla^2 T - \hat{u} \cdot \nabla T = \kappa_1 \frac{\partial^2 T}{\partial x^2} + \kappa_2 \frac{\partial^2 T}{\partial y^2} + \kappa_3 \frac{\partial^2 T}{\partial z^2} \qquad \text{(Eq 17)}$$

where the velocity vector $\hat{u}$ specifies the material flow field. NABF and ESD parameterization using this representation was applied in reference [13] for modeling friction stir welding processes.

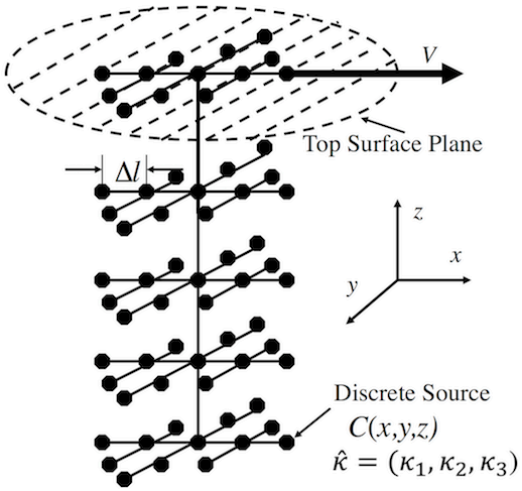

Fig. 1. Equivalent-source distribution, where discrete sources are distributed volumetrically, having specified strengths and effective-diffusion vectors.

Calculation of temperature histories using the parametric modeling methodology defined above entails adjustment of parameters $C(\hat{x}_k)$, $\hat{x}_k$, and $\hat{\kappa} = (\kappa_1, \kappa_2, \kappa_3)$, which define the ESD. The effective-diffusion vector is such that κ_1 is the thermal diffusivity of the workpiece, which is physically consistent with downstream heat

diffusion. In contrast, effective-diffusivity components κ_2 and κ_3 can be phenomenological adjustable parameters, which do not represent pure heat diffusion within the workpiece, but rather the combination of diffusion and advection.

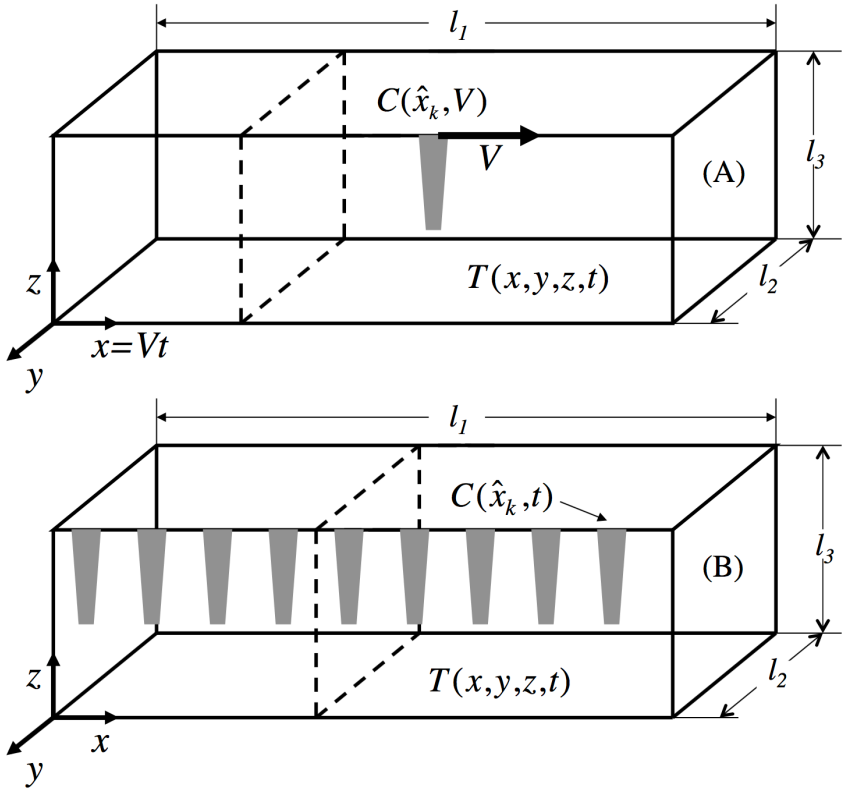

Fig. 2. Schematic representation of equivalent sources for steady state and time-dependent conditions.

Numerical-Analytical Basis Functions (Steady-State Conditions)

The basis functions given in this section are for a frame of reference that is fixed to a moving source distribution, representing the quasi-steady-state condition for energy deposition (see Fig. 2 top). These basis functions are composed of various combinations of the fundamental and Fourier series solutions to the heat conduction equation, and numerical integrations over discrete source distributions and time. These basis functions extend the inverse-analysis methodology for consideration of different types of boundary conditions on the workpiece, as well as different volumetric characteristics of energy-deposition within a workpiece.

Following the inverse analysis approach [1-8], parametric models provide a means for the inclusion of information concerning the physical characteristics of a given energy deposition process. The process of energy deposition is characterized by at least one workpiece surface. Given the general trend features of temperature fields associated with energy-deposition processes, parametric representations of temperature fields within structures characterized by a surface or finite thickness and width, in terms of numerical-analytical basis functions, are

$$T(\hat{x}) = T_A + \sum_{k=1}^{N_k}\sum_{n=1}^{N_t} C(\hat{x}_k) G_M(\hat{x}, \hat{x}_k, n\Delta t, \hat{\kappa}, V) \qquad \text{(Eq 18)}$$

where

$$G_1(\hat{x}, \hat{x}_k, t, \hat{\kappa}, V) = \frac{1}{\sqrt{t}}\exp\left[-\frac{(x - x_k - Vt)^2}{4\kappa_1 t}\right] \times \frac{1}{\sqrt{t}}\exp\left[-\frac{(y - y_k)^2}{4\kappa_2 t}\right] \times \frac{1}{\sqrt{t}}\exp\left[-\frac{(z - z_k)^2}{4\kappa_3 t}\right] \qquad \text{(Eq 19)}$$

$$G_2(\hat{x}, \hat{x}_k, t, \hat{\kappa}, V) = \frac{1}{\sqrt{t}}\exp\left[-\frac{(x - x_k - Vt)^2}{4\kappa_1 t}\right] \times \frac{1}{\sqrt{t}}\exp\left[-\frac{(y - y_k)^2}{4\kappa_2 t}\right] \times \left\{1 + 2\sum_{m=1}^{\infty}\exp\left[-\frac{\kappa_3 m^2 \pi^2 t}{l_3^2}\right]\cos\left[\frac{m\pi z}{l_3}\right]\cos\left[\frac{m\pi z_k}{l_3}\right]\right\} \qquad \text{(Eq 20)}$$

$$G_3(\hat{x}, \hat{x}_k, t, \hat{\kappa}, V) = \frac{1}{\sqrt{t}}\exp\left[-\frac{(x - x_k - Vt)^2}{4\kappa_1 t}\right] \times \left\{1 + 2\sum_{m=1}^{\infty}\exp\left[-\frac{\kappa_2 m^2 \pi^2 t}{l_2^2}\right]\cos\left[\frac{m\pi y}{l_2}\right]\cos\left[\frac{m\pi y_k}{l_2}\right]\right\} \times \left\{1 + 2\sum_{m=1}^{\infty}\exp\left[-\frac{\kappa_3 m^2 \pi^2 t}{l_3^2}\right]\cos\left[\frac{m\pi z}{l_3}\right]\cos\left[\frac{m\pi z_k}{l_3}\right]\right\} \qquad \text{(Eq 21)}$$

$$T(\hat{x}) = T_A + \sum_{k=1}^{N_k} C(\hat{x}_k) G_4(\hat{x}, \hat{x}_k, \hat{\kappa}, V) \qquad \text{(Eq 22)}$$

where

$$G_4(\hat{x}, \hat{x}_k, \hat{\kappa}, V) = \frac{1}{r} \exp\left[-\frac{V}{2} YY\right] \left(\sum_{n=1}^{N_t} F(z, z_k, n\Delta t, \kappa_3) \right), \quad \text{(Eq 23)}$$

$$F(z, z_k, t, \kappa_3) = 1 + 2 \sum_{m=1}^{\infty} \exp\left[-\frac{\kappa_3 \, m^2 \pi^2 t}{l_3^2}\right] \cos\left[\frac{m\pi z}{l_3}\right] \cos\left[\frac{m\pi z_k}{l_3}\right] \quad \text{(Eq 24)}$$

$$r = \sqrt{(x - x_k)^2 + (y - y_k)^2} \quad \text{(Eq 25)}$$

$$YY = \sqrt{\frac{(x - x_k)^2}{{\kappa_1}^2} + \frac{(y - y_k)^2}{{\kappa_2}^2}} + \left(\frac{x - x_k}{\kappa_1}\right) \quad \text{(Eq 26)}$$

$$T(\hat{x}) = T_A + \sum_{k=1}^{N_k} C(\hat{x}_k) G_5(\hat{x}, \hat{x}_k, \hat{\kappa}, V) \quad \text{(Eq 27)}$$

$$G_5(\hat{x}, \hat{x}_k, \hat{\kappa}, V) = \frac{1}{r} \exp\left[-\frac{V}{2} XX\right] \quad \text{(Eq 28)}$$

where

$$r = \sqrt{(x - x_k)^2 + (y - y_k)^2 + (z - z)^2} \quad \text{(Eq 29)}$$

$$XX = \sqrt{\frac{(x - x_k)^2}{{\kappa_1}^2} + \frac{(y - y_k)^2}{{\kappa_2}^2} + \frac{(z - z_k)^2}{{\kappa_3}^2}} + \left(\frac{x - x_k}{\kappa_1}\right) \quad \text{(Eq 30)}$$

$$T(\hat{x}) = T_A + \sum_{k=1}^{N_k} C(\hat{x}_k) G_6(\hat{x}, \hat{x}_k, \hat{\kappa}, V) \quad \text{(Eq 31)}$$

where

$$G_6(\hat{x}, \hat{x}_k, \hat{\kappa}, V) = \exp\left[-\frac{V}{2\kappa_1}(x - x_k)\right] K_0\left(\frac{V}{2} ZZ\right) \quad \text{(Eq 32)}$$

$$ZZ = \sqrt{\frac{(x - x_k)^2}{{\kappa_1}^2} + \frac{(y - y_k)^2}{{\kappa_2}^2}} \quad \text{(Eq 33)}$$

and $C(\hat{x}_k)$ is the discrete-source function value at $\hat{x}_k$. The quantities $\hat{\kappa} = (\kappa_1, \kappa_2, \kappa_3)$, V, l_2 and l_3 are the diffusivity vector, energy-deposition speed, plate width and thickness, respectively.

The inverse analysis methodology combines numerical integration with optimization of linear combinations of numerical-analytical basis functions. Equation (1) includes a discrete numerical integration over time, where the time step Δt is specified according to the average energy deposited during the time Δt. The inverse analysis methodology defined above is equipped with a mathematical structure that satisfies all boundary conditions associated with energy-deposition within plate structures [4-11].

A length scale parameter l_S, where $l_S < l_1$, l_2, and l_3, is adopted for specification of the spatial scale of the calculated temperature field with respect to which parameters are adjusted. This length scale parameter provides for inclusion of more details of shape features of measured temperature-field boundaries to be adopted as constraint conditions. Accordingly, the inverse analysis methodology adopts three types of length parameters l_S, l_1, l_2, and l_3. These are: length pararmeters corresponding to actual physical dimensions of the workpiece, length pararmeters specifying finite-workpiece or far-field boundary conditions; and the length parameter l_S, which specifies the local region of the temperature field to be calculated (see reference [4]).

As indicated previously, different formulations of numerical-analytical basis functions are significant in that they provide for the inclusion of different types of workpiece boundary conditions and energy-deposition shape features relative to the region of interest for calculation of temperature fields.

In that the inverse-thermal-analysis methodology involves adjustment of equivalent source distributions, the linear combinations of numerical-analytical basis functions, defined for steady state and time-dependent processes, can be extended to include time-delay parameters t_d such that the time variable t is replaced by $t+t_d$. Following the inverse thermal analysis approach, fine details of spatial and temporal characteristics of the energy source are not relevant to those of the temperature field within regions of interest at far field.

Numerical-Analytical Basis Functions (Time-Dependent Conditions)

The basis functions given in this section consider energy deposition for a frame of reference that is fixed to the workpiece (see Fig. 2 bottom). These basis functions can be used for inverse modeling of unsteady time-dependent heat-deposition processes. Such conditions can be associated with start-and-stop influence of energy deposition, as well as the finite length of a workpiece along the direction of energy deposition. For time-dependent energy-deposition processes, parametric representation of temperature fields within finite volumes of materials, in terms of numerical-analytical basis functions, are

$$T(\hat{x},t) = T_A + \sum_{k=1}^{N_k}\sum_{n=1}^{N_t} C(\hat{x}_k, n\Delta t - t_k) G_M(\hat{x}, \hat{x}_k, \hat{\kappa}, n\Delta t - t_k) \qquad \text{(Eq 34)}$$

where

$$G_7(\hat{x}, \hat{x}_k, t - t_k, \hat{\kappa}) = \frac{1}{\sqrt{(t-t_k)}}\exp\left[-\frac{(x-x_k)^2}{4\kappa_1(t-t_k)}\right] \times \frac{1}{\sqrt{(t-t_k)}}\exp\left[-\frac{(y-y_k)^2}{4\kappa_2(t-t_k)}\right]$$

$$\times \frac{1}{\sqrt{(t-t_k)}}\exp\left[-\frac{(z-z_k)^2}{4\kappa_3(t-t_k)}\right], \qquad \text{(Eq 35)}$$

$$G_8(\hat{x}, \hat{x}_k, t - t_k, \hat{\kappa}) = \frac{1}{\sqrt{(t-t_k)}}\exp\left[-\frac{(x-x_k)^2}{4\kappa_1(t-t_k)}\right] \times \frac{1}{\sqrt{(t-t_k)}}\exp\left[-\frac{(y-y_k)^2}{4\kappa_2(t-t_k)}\right]$$

$$\times\left\{1 + 2\sum_{m=1}^{\infty}\exp\left[-\frac{\kappa_3 m^2\pi^2(t-t_k)}{l_3^2}\right]\cos\left[\frac{m\pi z}{l_3}\right]\cos\left[\frac{m\pi z_k}{l_3}\right]\right\}, \qquad \text{(Eq 36)}$$

$$G_9(\hat{x}, \hat{x}_k, t - t_k, \hat{\kappa}) = \frac{1}{\sqrt{(t-t_k)}}\exp\left[-\frac{(x-x_k)^2}{4\kappa_1(t-t_k)}\right] \times\left\{1 + 2\sum_{m=1}^{\infty}\exp\left[-\frac{\kappa_2 m^2\pi^2(t-t_k)}{l_2^2}\right]\cos\left[\frac{m\pi y}{l_2}\right]\cos\left[\frac{m\pi y_k}{l_2}\right]\right\}$$

$$\times\left\{1 + 2\sum_{m=1}^{\infty}\exp\left[-\frac{\kappa_3 m^2\pi^2(t-t_k)}{l_3^2}\right]\cos\left[\frac{m\pi z}{l_3}\right]\cos\left[\frac{m\pi z_k}{l_3}\right]\right\}, \qquad \text{(Eq 37)}$$

and

$$G_{10}(\hat{x},\hat{x}_k,t-t_k,\hat{\kappa}) = \left\{1+2\sum_{m=1}^{\infty}\exp\left[-\frac{\kappa_1 m^2\pi^2(t-t_k)}{l_1^2}\right]\cos\left[\frac{m\pi x}{l_1}\right]\cos\left[\frac{m\pi x_k}{l_1}\right]\right\}$$

$$\times\left\{1+2\sum_{m=1}^{\infty}\exp\left[-\frac{\kappa_2 m^2\pi^2(t-t_k)}{l_2^2}\right]\cos\left[\frac{m\pi y}{l_2}\right]\cos\left[\frac{m\pi y_k}{l_2}\right]\right\}$$

$$\times\left\{1+2\sum_{m=1}^{\infty}\exp\left[-\frac{\kappa_3 m^2\pi^2(t-t_k)}{l_3^2}\right]\cos\left[\frac{m\pi z}{l_3}\right]\cos\left[\frac{m\pi z_k}{l_3}\right]\right\} \qquad \text{(Eq 38)}$$

The time-dependent source and time are given, respectively, by

$$C(\hat{x}_k,t_k,t) = C(\hat{x}_k)u(t-t_k)\ , \qquad \text{(Eq 39)}$$

and

$$t = N_t\Delta t \qquad \text{(Eq 40)}$$

The quantitie $C(\hat{x}_k)$, $\hat{\kappa} = (\kappa_1,\kappa_2,\kappa_3)$, V, l_2 and l_3 are as defined above. The quantity l_1 specifies the length of the workpiece along the direction of energy deposition. The procedure for inverse analysis using basis functions given above entails adjustment of the parameters $C(\hat{x}_k)$, $\hat{x}_k$, t_k and Δt defined over the entire spatial region of the workpiece. Formally, this procedure entails adjustment of the time-dependent temperature field defined over the entire spatial region of the sample volume.

Numerical-Analytical Basis Functions (Advection)

Another set of basis functions considers parametric modeling of energy deposition by explicit phenomenological representation of advective influences. For the representation, the concept of effective-diffusion vectors is extended to that of effective-advection vectors. For time-dependent energy-deposition processes, parametric representations using NABFs of temperature fields, characterized by advective features, are

$$T(\hat{x},t) = T_A + \sum_{k=1}^{N_k}\sum_{n=1}^{N_t} C(\hat{x}_k, n\Delta t - t_k)G_M(\hat{x},\hat{x}_k,\hat{\kappa}_k,\hat{V}_k,n\Delta t - t_k) \qquad \text{(Eq 41)}$$

where $$\hat{V}_k = (V_{1k}, V_{2k}, V_{3k}),$$ (Eq 42)

and

$$G_{11}(\hat{x}, \hat{x}_k, \hat{\kappa}_k, \hat{V}_k, n\Delta t - t_k) = \frac{1}{\sqrt{(t-t_k)}} \exp\left[-\frac{(x - x_k - V_{1k}(t-t_k))^2}{4\kappa_{1k}(t-t_k)}\right]$$
$$\times \frac{1}{\sqrt{(t-t_k)}} \exp\left[-\frac{(y - y_k - V_{2k}(t-t_k))^2}{4\kappa_{2k}(t-t_k)}\right]$$
$$\times \frac{1}{\sqrt{(t-t_k)}} \exp\left[-\frac{(z - z_k - V_{3k}(t-t_k))^2}{4\kappa_{3k}(t-t_k)}\right] \quad \text{(Eq 43)}$$

$$G_{12}(\hat{x}, \hat{x}_k, \hat{\kappa}_k, \hat{V}_k, n\Delta t - t_k) = \frac{1}{\sqrt{(t-t_k)}} \exp\left[-\frac{(x - x_k - V_{1k}(t-t_k))^2}{4\kappa_{1k}(t-t_k)}\right]$$
$$\times \frac{1}{\sqrt{(t-t_k)}} \exp\left[-\frac{(y - y_k - V_{2k}(t-t_k))^2}{4\kappa_{2k}(t-t_k)}\right]$$
$$\times \left\{1 + 2\sum_{m=1}^{\infty} \exp\left[-\frac{\kappa_3 m^2 \pi^2 (t-t_k)}{l_3^2}\right] \cos\left[\frac{m\pi z}{l_3}\right] \cos\left[\frac{m\pi z_k}{l_3}\right]\right\} \quad \text{(Eq 44)}$$

$$G_{13}(\hat{x}, \hat{x}_k, \hat{\kappa}_k, \hat{V}_k, n\Delta t - t_k) = \frac{1}{\sqrt{(t-t_k)}} \exp\left[-\frac{(x - x_k - V_{1k}(t-t_k))^2}{4\kappa_{1k}(t-t_k)}\right]$$
$$\times \left\{1 + 2\sum_{m=1}^{\infty} \exp\left[-\frac{\kappa_2 m^2 \pi^2 (t-t_k)}{l_2^2}\right] \cos\left[\frac{m\pi y}{l_2}\right] \cos\left[\frac{m\pi y_k}{l_2}\right]\right\}$$
$$\times \frac{1}{\sqrt{(t-t_k)}} \exp\left[-\frac{(z - z_k - V_{3k}(t-t_k))^2}{4\kappa_{3k}(t-t_k)}\right] \quad \text{(Eq 45)}$$

Equation (42) defines the effective-advection vector.

Discussion

The NABFs defined above, for inverse thermal analysis of steady-state and time-dependent heat deposition, are to be applied by a general procedure that tends toward minimal complexity and computational cost. This procedure entails construction of ESDs with respect to specified local regions (or locations) of temperature-history sampling. Accordingly, computational cost scales with ESD size only, and not with spatial characteristics of the workpiece, as for inverse analysis procedures based on Finite Elements and Finite Differences. Following the inverse-analysis approach, effective-diffusivity and effective-advection vectors are space-time-average quantities, representing the combined influence of diffusion, advection and energy-coupling characteristics associted with a given heat-deposition process, to be determined and not assumed *a priori*. In addition, influences of nonconducting boundaries (or surfaces) and far-field source distributions, whose "details" have no influence, are modeled parametrically. As should be emphasized, the methodology presented here seeks prediction of temperature fields for heat-deposition processes by inverse analysis using parametric models. This approach should be well posed in that heat-deposition processes, no matter their complexity, tend to fall within classes having associated specific characteristics, e.g., welding processes of various types. Thus, NABFs and ESDs should provide optimal parameterization of these characteristics, which should be for construction of parameters spaces, and prediction of temperature fields by interpolation within these spaces. The inverse analysis methodology considered here can be applied (in principle) to both laboratory measurements and results of numerical simulations using physics based models, i.e., computational experiments. The perspective of appying, in principle, inverse thermal analysis to both numerical-model simulations and laboratory measurements, emphasizes the distinction of this methodology with respect to approach.

The methodology presented here can be catergorized as based on "pure" inverse analysis, which is in terms of characteristic modes of heat-deposition, i.e., NABFs. It is distinct from methodologies combining inverse analysis with elements of direct modeling, which include detailed physical representaions, e.g., temperature dependence of thermal diffusivity. For this methodology, material properties are adopted as parameters only when

they represent well defined constraints on the calculated temperature field, e.g., effective-diffusion-vector component κ_1 representing downstream heat diffusion within a workpiece.

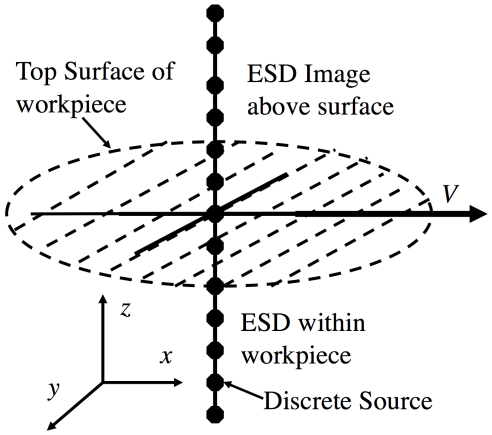

Fig. 3. Equivalent source distribution applying nonconducting boundary condition at workpiece surface.

Inverse thermal analysis using NABFs described in this report assumes that temperature gradients are only appreciable within regions of energy deposition, no matter the size or geometric complexity of workpieces. Accordingly, the time-dependennt temperature field within a workpiece, having a relative complex shape, resulting from energy deposition at different locations and times, can be decomposed into near and far-field components. Near field components are modeled using NABFs, which includes the influence of boundaries within close proximity of deposition, while far field components are modeled as background contributions having relatively small gradients. Shown in Fig. 3 is representation of a procedure for applying nonconducting boundary conditions using the NABFs defined by Eqs. (19), (35) and (43).

Conclusion

The objective of this report is to present a collection of basis functions extending an inverse thermal analysis methodology with respect to its formulation. This methodology, using numerical-analytical basis functions (NABFs) and equivalent source distributions (ESDs), adopts the analysis approach of signal processing [1], where

a system's response is modeled using linear combinations of component contributions, which are characteristic modes of that system. Further analysis is needed concerning algorithm development for application of the parametric models described here. Finally, these models should be used for inverse thermal analysis of different types of energy-deposition processes.

Acknowledgement

This work was supported by a Naval Research Laboratory (NRL) internal core program.

References

1. S.G. Lambrakos, "Parametric Modeling of Welding Processes Using Numerical-Analytical Basis Functions and Equivalent Source Distributions," Journal of Materials Engineering and Performance, Volume 25(4), April 2016, pp. 1360-1375.
2. S.G**.** Lambrakos and S.G. Michopoulos, Algorithms for Inverse Analysis of Heat Deposition Processes, 'Mathematical Modelling of Weld Phenomena,' Volume 8, 847, Published by Verlag der Technischen Universite Graz, Austria (2007).
3. S.G. Lambrakos and J.O. Milewski, Analysis of Welding and Heat Deposition Processes using an Inverse-Problem Approach, Mathematical Modelling of Weld Phenomena, **7**, 1025, Publishied by Verlag der Technischen Universite Graz, Austria 2005, pp. 1025-1055.
4. S.G. Lambrakos, "Inverse Thermal Analysis of 304L Stainless Steel Laser Welds," J. Mater. Eng. And Perform., 22(8), 2141 (2013).
5. S.G. Lambrakos, "Inverse Thermal Analysis of Stainless Steel Deep-Penetration Welds Using Volumetric Constraints," Journal of Materials Engineering and Performance, Volume 23(6), June 2014, pp. 2219-2232.

6. S.G. Lambrakos, “Inverse Thermal Analysis of Welds Using Multiple Constraints and Relaxed Parameter Optimization,” Journal of Materials Engineering and Performance, Volume 24(8) August 2015, pp. 2925-2936.
7. S.G. Lambrakos, A. Shabaev, L. Huang, “Inverse Thermal Analysis of Titanium GTA Welds Using Multiple Constraints,” Journal of Materials Engineering and Performance, Volume 24(6), June 2015, pp. 2401-2411.
8. S.G. Lambrakos, A. Shabaev, “Temperature Histories of Ti-6Al-4V Pulsed-Mode Laser Welds Calculated Using Multiple Constraints,” Naval Research Laboratory Memorandum Report, Naval Research Laboratory, Washington, DC, NRL/MR/6390--15-9621 (August 12, 2015).
9. D. Rosenthal, “The theory of moving sources of heat and its application to metal treatments,” Trans ASME, Vol. 68 (1946), pp. 849-866.
10. O. Grong, “Metallurgical Modelling of Welding,” 2ed., Materials Modelling Series, (H.K.D.H. Bhadeshia, ed.), published by The Institute of Materials, UK, (1997), chapter 2: pp. 1-115.
11. R.O. Myhr and O. Grong,’Acta Metall. Mater., 38, 1990, pp. 449-460.
12. H. S. Carslaw and J. C. Jaegar: Conduction of Heat in Solids, Clarendon Press, Oxford, 2nd ed, 374, 1959.
13. S.G. Lambrakos, “Parametric Modeling of AZ31-Mg Alloy Friction Stir Weld Temperature Histories,” J. Mater. Eng. And Perform., 27(11), (2018), pp. 5823-5830.

Appendix 1: Solutions of Heat Conduction Equation for Numerical-Analytical Basis Functions

Given here are different forms of solution to the time-dependent heat conduction equation, useful for construction of numerical-analytical basis functions. Different forms of solution to the one-dimensional heat conduction equation

$$\frac{\partial T(x,t)}{\partial t} = \kappa \frac{\partial^2 T(x,t)}{\partial x^2} \qquad \text{(Eq 46)}$$

with initial condition

$$T(x,0) = C_k \delta(x - x_k) \ , \qquad \text{(Eq 47)}$$

are the *Fourier Series Solution* (See Fig, 4A)

$$T(x,t) = \frac{C_k}{L}\left\{1 + 2\sum_{k=1}^{\infty} \exp\left(-\kappa \frac{4\pi^2 k^2 t}{L^2}\right) \cos\left[\frac{2\pi k(x - x_k)}{L}\right]\right\}, \qquad \text{(Eq 48)}$$

the *Kernel Solution* Eq. (11) (see Fig. 4B) and the *Fourier Series Solution for Nonconducting Boundaries* Eq.(12), which follows from Eq.(48). Using Eq.(48), one specifies the region of the temperature field to be within half the period L of the solution, where $L=2l$. The periodicity of this function permits construction of nonconducting boundary conditions at $x = 0$ and $x = l$ for any given source at $x = x_k$, by placement of image sources at $x = - x_k$, $L - x_k$ and $L + x_k$ (see Fig. 4C). For this combination of source and image locations, the temperature field within the region $[0,l]$ is given by

$$T(x,t) = \frac{C_k}{L}\left\{1 + 2\sum_{k=1}^{\infty} \exp\left(-\kappa \frac{4\pi^2 k^2 t}{L^2}\right) f(x,x_k)\right\} \qquad \text{(Eq. 49)}$$

where

$$f(x,x_k) = \cos\left[\frac{2\pi k(x - x_k)}{L}\right] + \cos\left[\frac{2\pi k(x + x_k)}{L}\right]$$

$$+ \cos\left[\frac{2\pi k(x - L + x_k)}{L}\right] + \cos\left[\frac{2\pi k(x - L - x_k)}{L}\right] \qquad \text{(Eq. 50)}$$

Finally, noting that

$$f(x,x_k) = \cos\left[\frac{2\pi kx}{L}\right] \cos\left[\frac{2\pi kx_k}{L}\right], \qquad \text{(Eq. 51)}$$

letting $L = 2l$, and defining the region of the temperature field as shown in Fig. 4C, the solution for nonconducting boundaries follows.

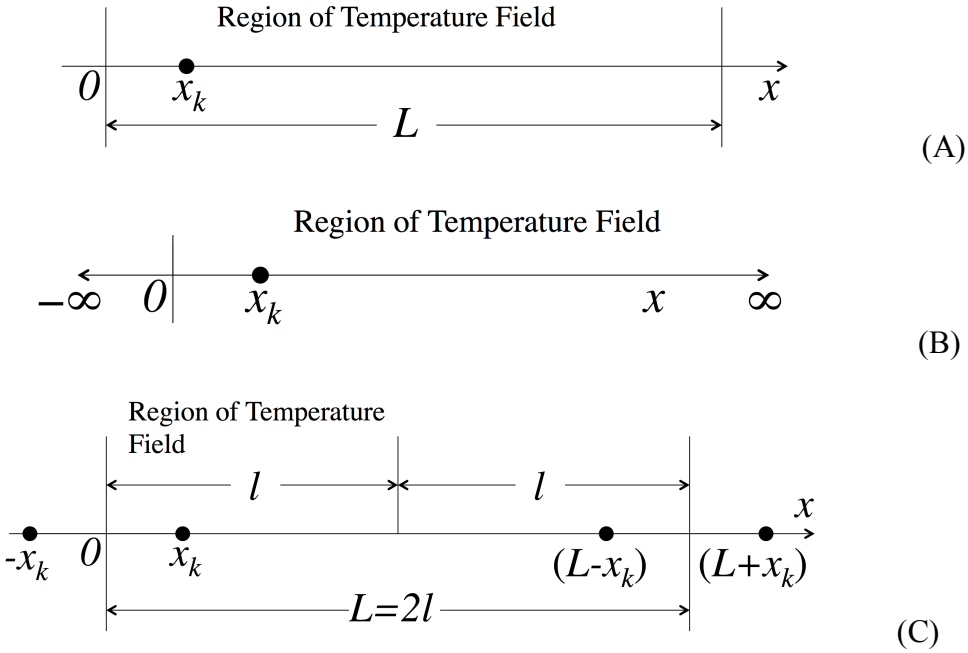

Fig 4. Schematic representation of temperature-field regions defined according to different forms of solutions for the heat conduction equation.